Supporting Information

Implications of Pyran Cyclization and Pterin Conformation on Oxidized forms of the Molybdenum Cofactor

Douglas R. Gisewhite[a], Jing Yang[b], Benjamin R. Williams[a], Alisha Esmail[a],

Benjamin Stein[b], Martin L. Kirk*[b], Sharon J. N. Burgmayer*[a]

[a]Department of Chemistry, Bryn Mawr College, Bryn Mawr, Pennsylvania 19010, USA; [b]Department of Chemistry and Chemical Biology, The University of New Mexico, MSC03 2060, 1 University of New Mexico, Albuquerque, New Mexico 87131-0001, United States

Contents:

Figure S1. ^{1}H NMR spectrum of BDMPP in chloroform-d.
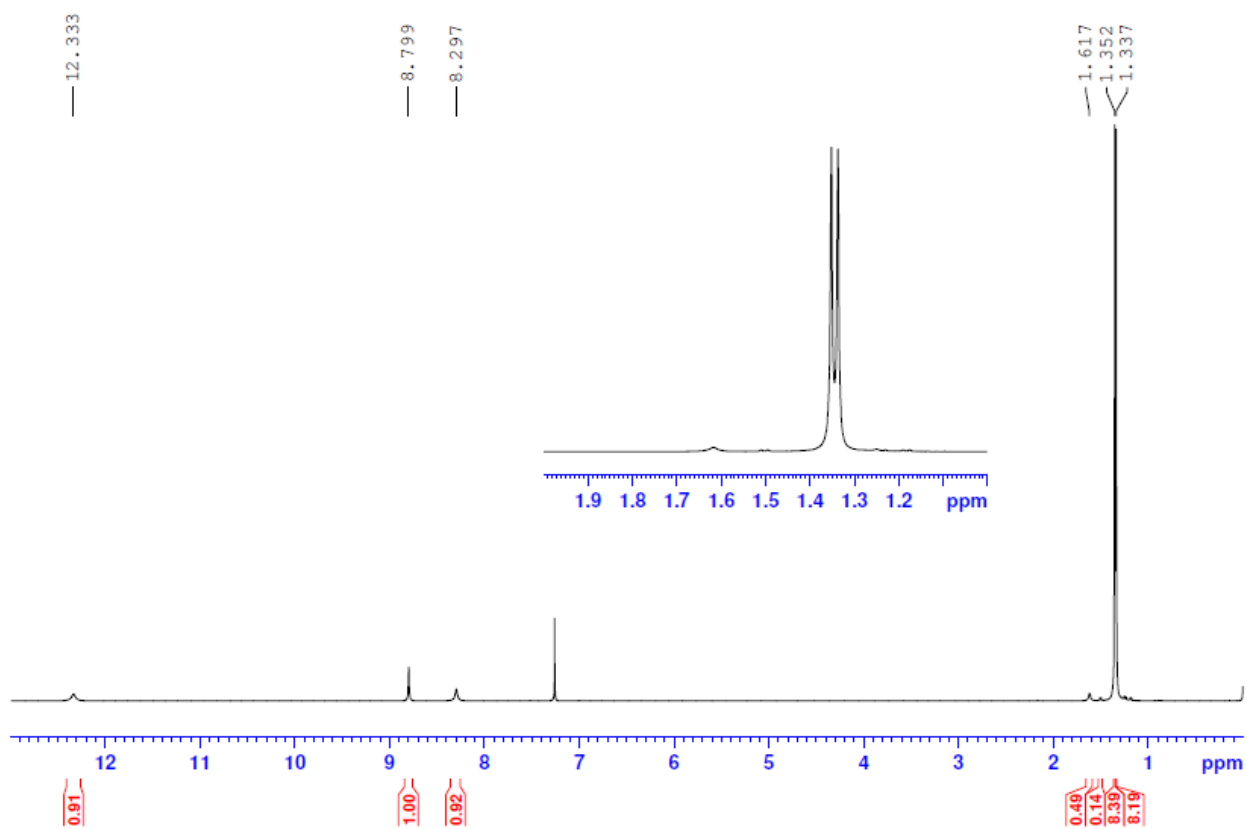
Figure S2. ^1H NMR spectrum of **2** in acetonitrile-d^3.
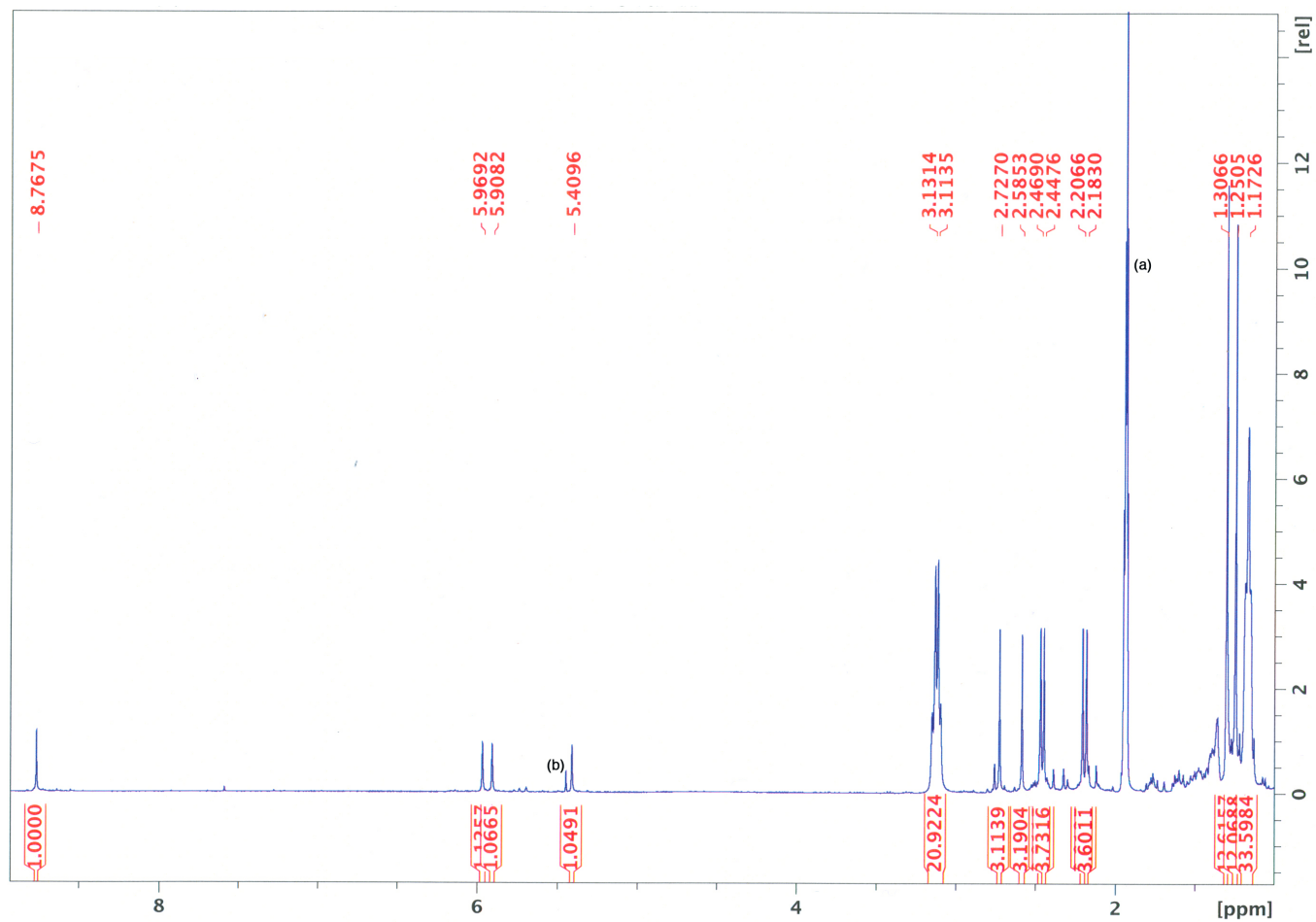
(a) Residual acetonitrile resonance
(b) Contaminant CH_2Cl_2

Figure S3. HSQC spectrum of **2** in chloroform-d.
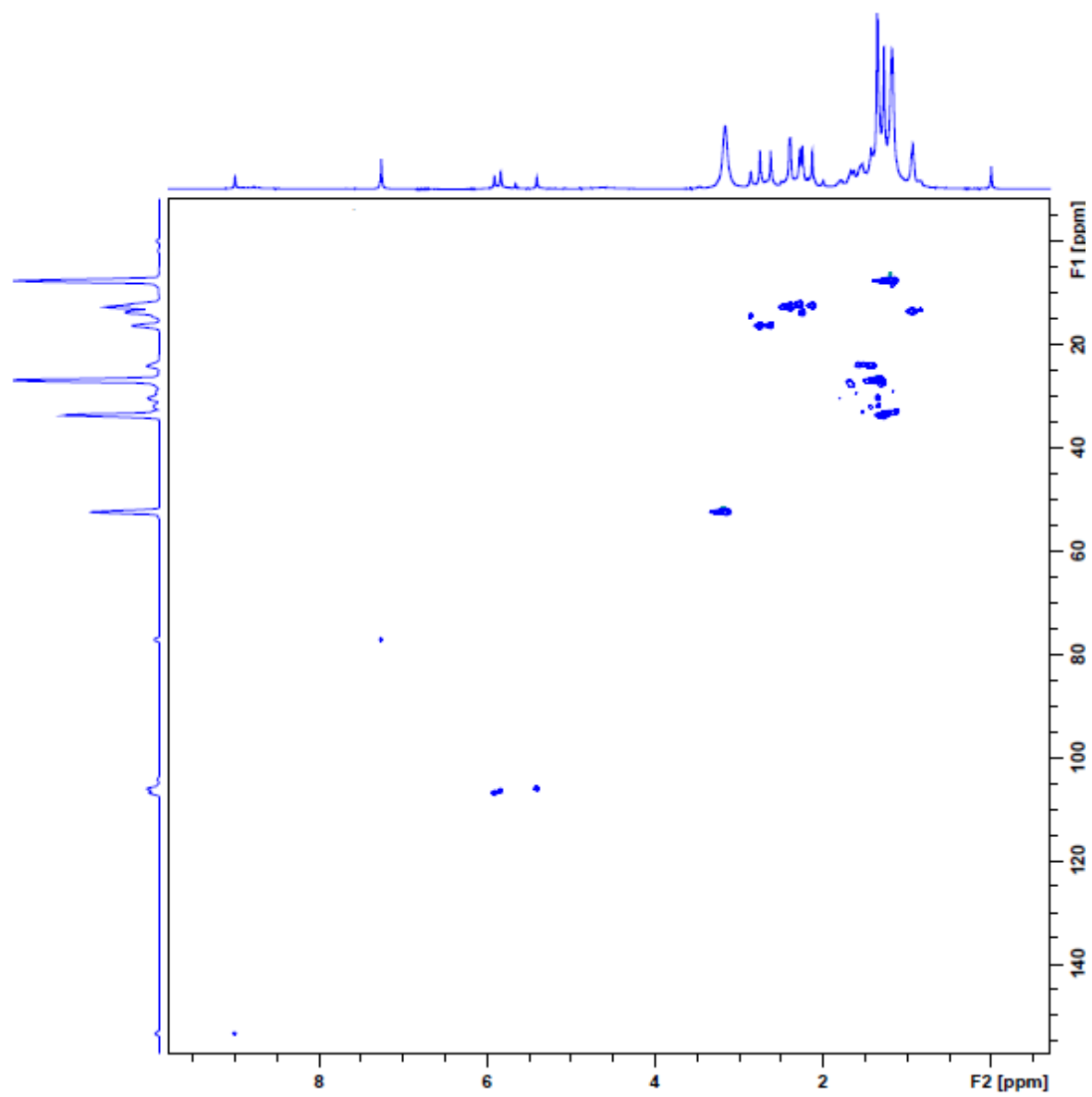
Figure S4. UV-vis overlay of **1** (blue) and **2** (red) in acetonitrile at 3.00 x 10^{-5} M.
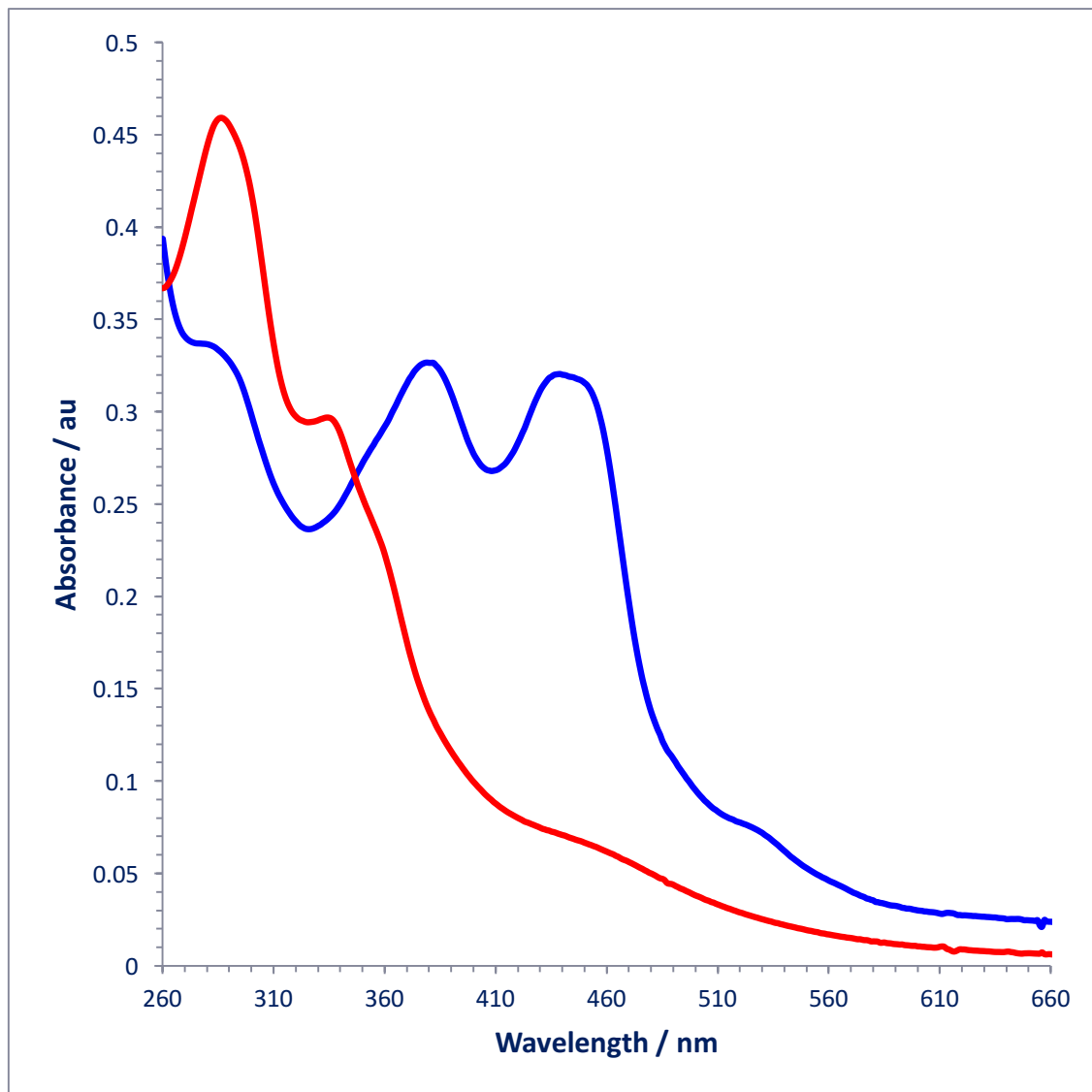
Figure S5. UV-vis overlay of **1** (blue) and **2** (bed) in CHCl$_3$ at 3.00 x 10^{-5} M.
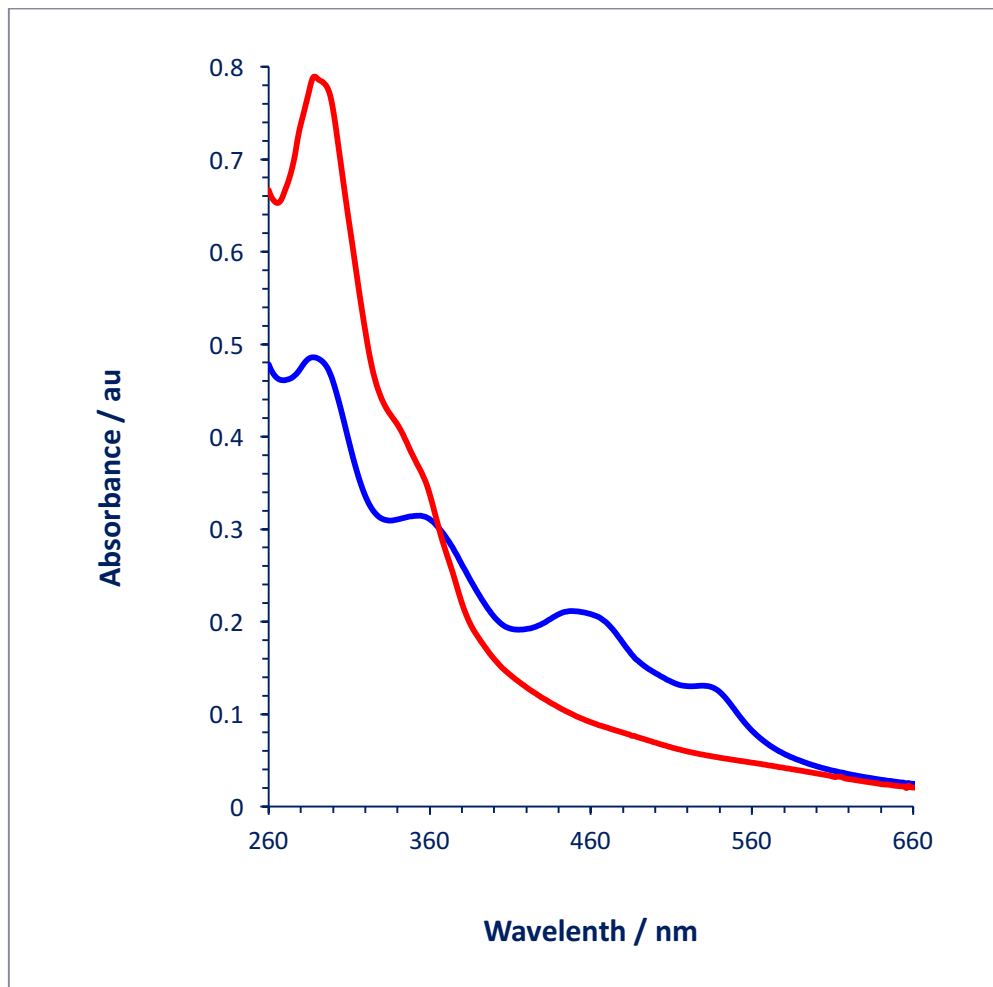
Figure S6. Computed charge transfer transitions for 2, including EDDMs that depict their dominant dithiolene → pterin ILCT character.
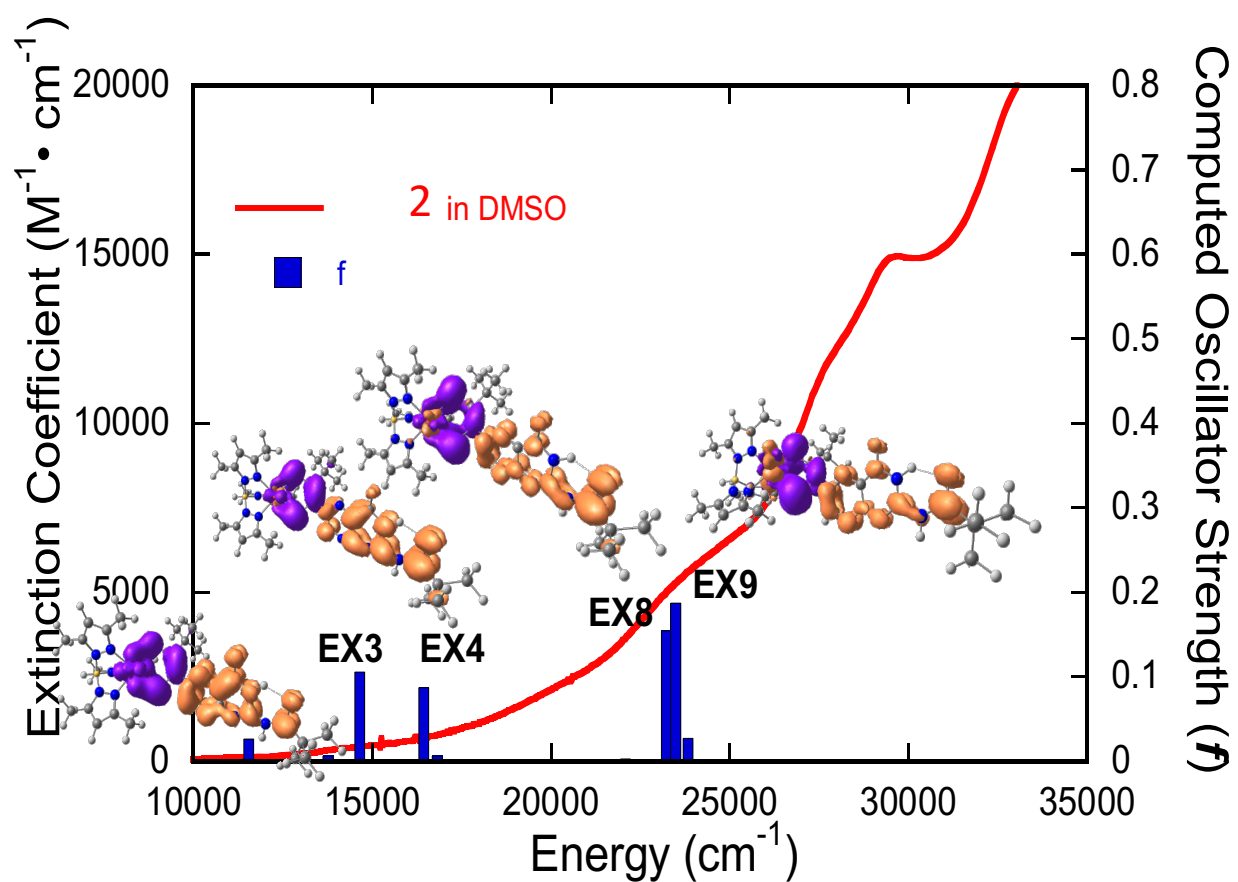
Figure S7. Mo K-edge XANES spectra for 1 and 2.
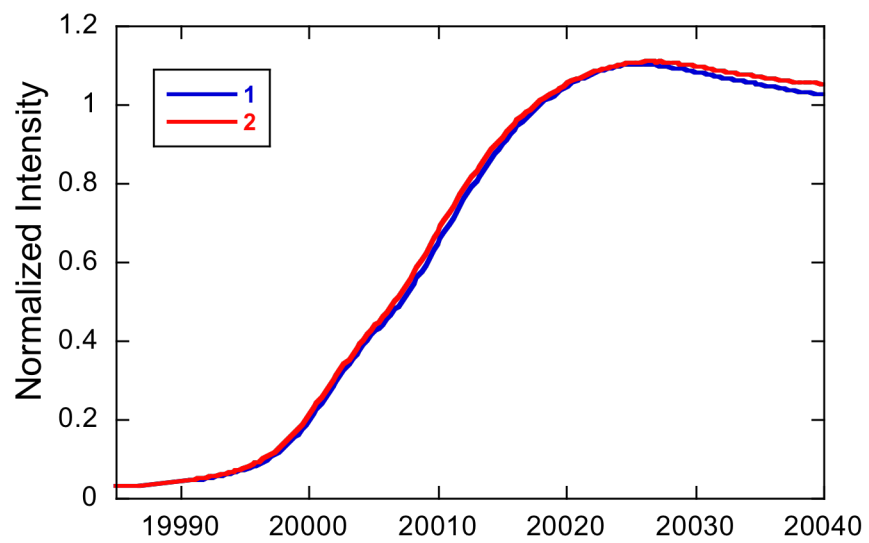
Figure S8. Cyclic **v**oltammogram **o**verlay of 1 (**b**lue) and 2 (**r**ed) in Chloroform.
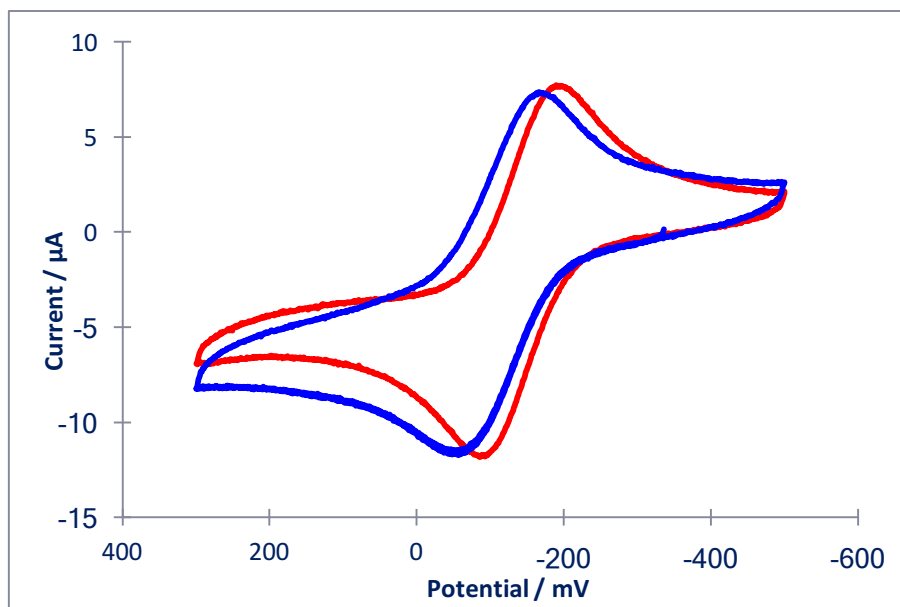
Cyclic voltammograms of **1** (blue) and **2** (red), in 0.10 M TBAP/CHCl$_3$ vs Ag/AgCl at a Pt working electrode, scan rate 100 mV/sec.

Table S1. Cyclic voltammetric data for **1** and **2** in dcetonitrile (ACN) and dhloroform (CHCl$_3$)

| Complex (solvent)	Scan rate, mV/s	E(1/2), mV [a]	p$_c$ – p$_a$, mV [b]	i$_c$ / i$_a$ [c]
1 (ACN)	25	-519	74	0.99
1 (ACN)	100	-520	74	0.99
1 (ACN)	400	-521	81	1.03
1 (ACN)	800	-520	89	0.96
2 (ACN)	25	-572	80	0.98
2 (ACN)	100	-574	83	0.96
2 (ACN)	400	-575	99	1.00
2 (ACN)	800	-573	100	1.05
1 (CHCl$_3$)	100	-621	115	0.98
2 (CHCl$_3$)	100	-650	108	0.97

[a] vs Fc+/Fc, +440 mV vs Ag/AgCl, (p$_c$ – p$_a$) = 73 mV in ACN; or +510 mV vs Ag/AgCl, (p$_c$ – p$_a$) = 100 mV in CHCl$_3$, 100 mV/sec

[b] difference between cathodic and anodic potentials

[c] ratio of cathodic to anodic currents

Figure S9. Cyclic **v**oltammograms under variable scan rate for 1 (top) and 2 (bottom) in acetonitrile, 0.1M TBAP, vs AgCl/Ag.
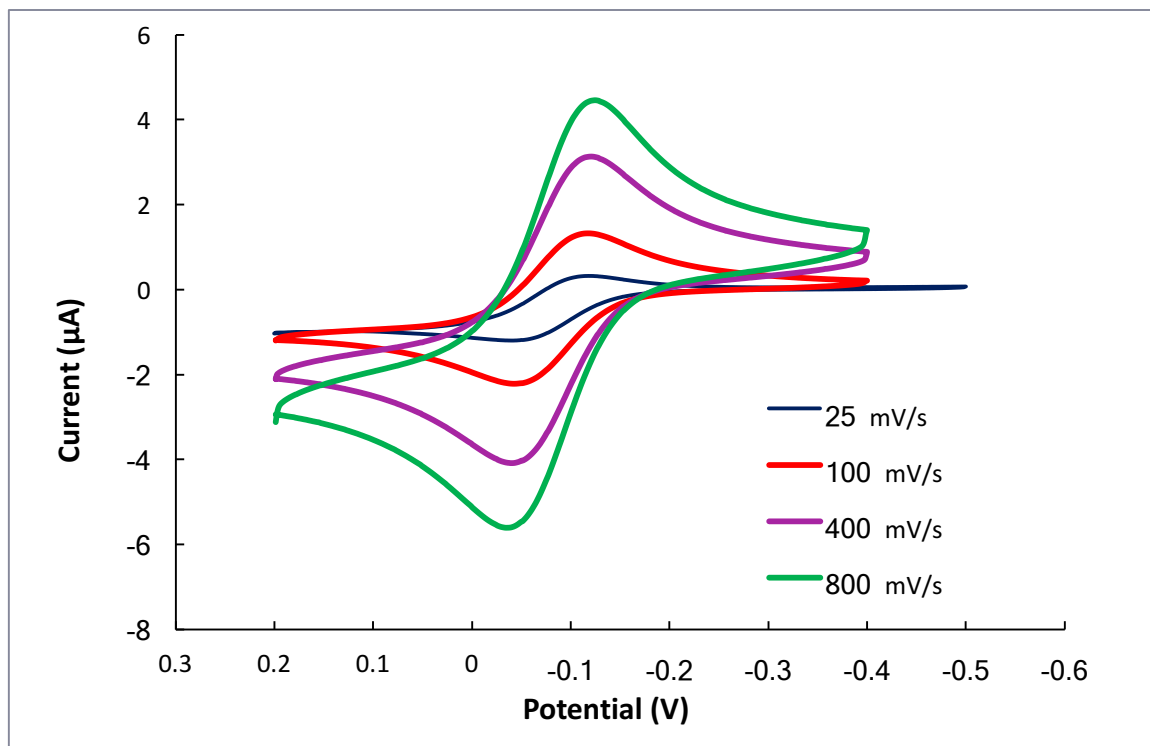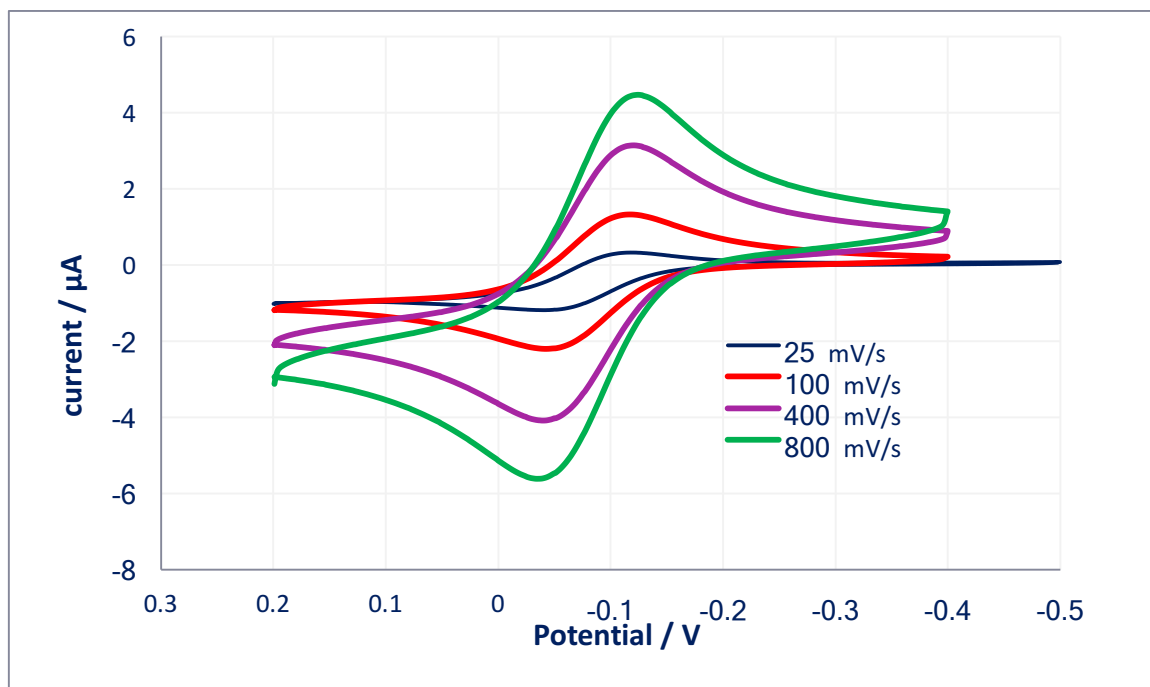
Figure S10. Illustration of pterin-dithiolene dihedral angle rotation of **2**.

Steric Clash
Pterin Dihedral Angle of -30^0

Steric Clash
Pterin Dihedral Angle of 160^0
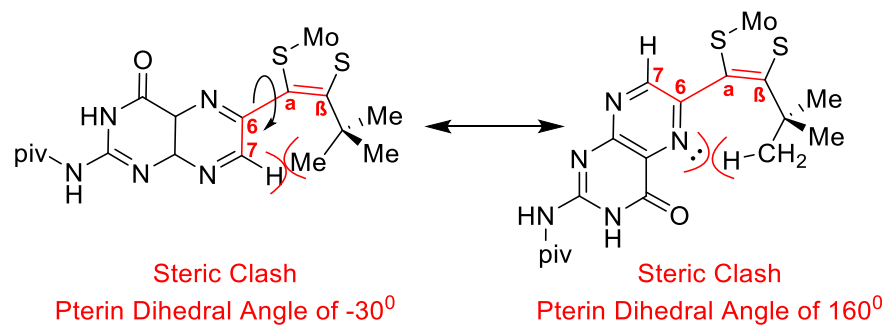
Calculated total energy as a function of rotation about the pterin-dithiolene bond in 2 (all other atoms remain frozen).
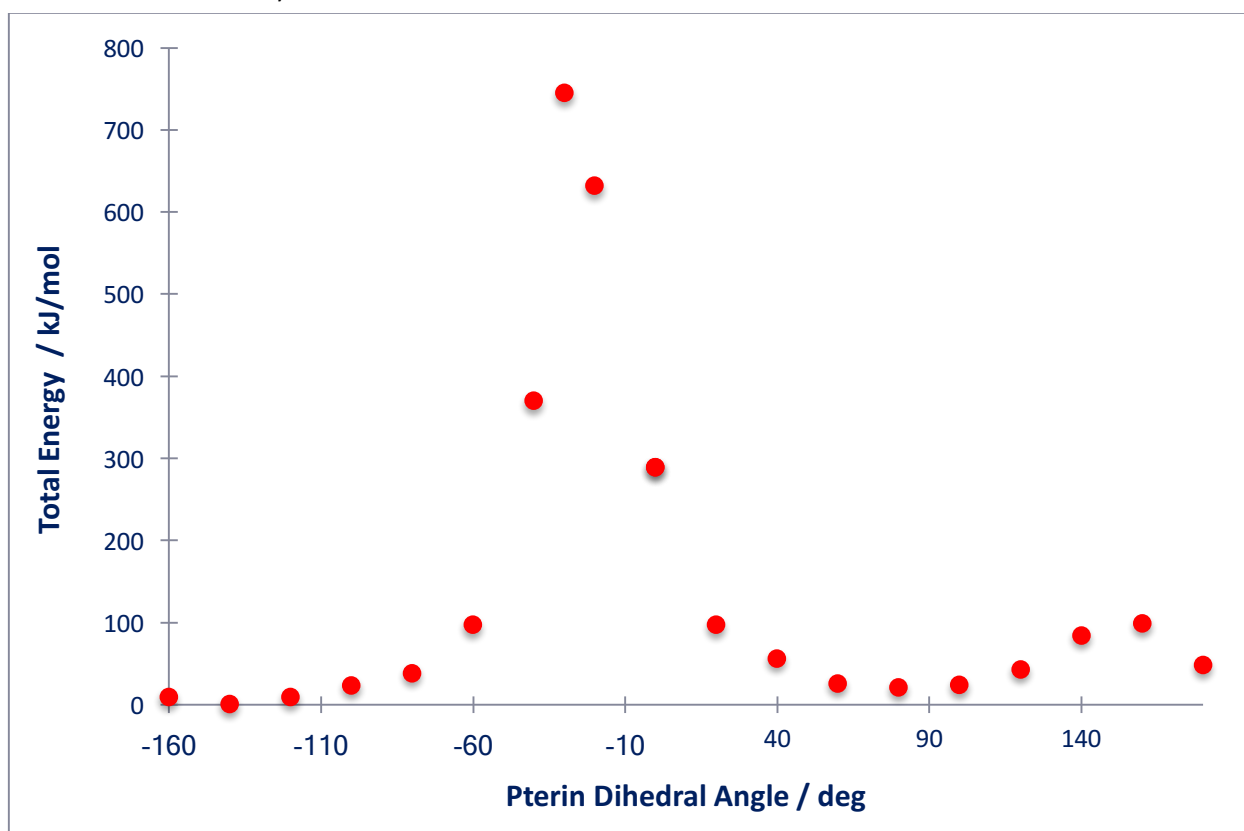
Table S2. Electronic absorption spectroscopy band assignments for **1**

Band	Energy (cm^{-1})	Oscillator Strength (Exp)	Oscillator Strength (Calc)	Band Assignment (one-electron promotions that contribute to individual transitions are grouped by number)
A	20,000	0.028	0.0052	1. H0(xy)→L0(pterin) (44%)
				1. H0(xy))→L+2(xz) (34%)
B	22,500	0.115	0.2676	1. H-1(dithiolene)→L0(pterin) (86%)
C	24,000	0.040	0.1429	1. H-1(dithiolene)→L+1(xz+pterin) (51%)
				1. H-1(dithiolene)→L+2(xz) (17%)
				2. H0(xy)→L+3(yz+Tp) (28%)
				2. H0(xy)→L+5(yz+Tp) (19%)
				2. H0(xy)→L+6(yz+Tp) (18%)
				3. H0(xy)→L+7(xz+pterin) (22%)
				3. H0(xy)→L+4(pterin) (22%)
D	26,000	0.196	0.4543	1. H-2(dithiolene)→L0(pterin) (80%)

Figure S11. EDDMs for bands A, C, and D in **1**. The purple regions represent an electron density loss in the transition and the orange regions represent an electron density gain in the transition. The LUMO, HOMO, HOMO-1, and HOMO-2 are given below.

Band A   **Band C**   **Band D**
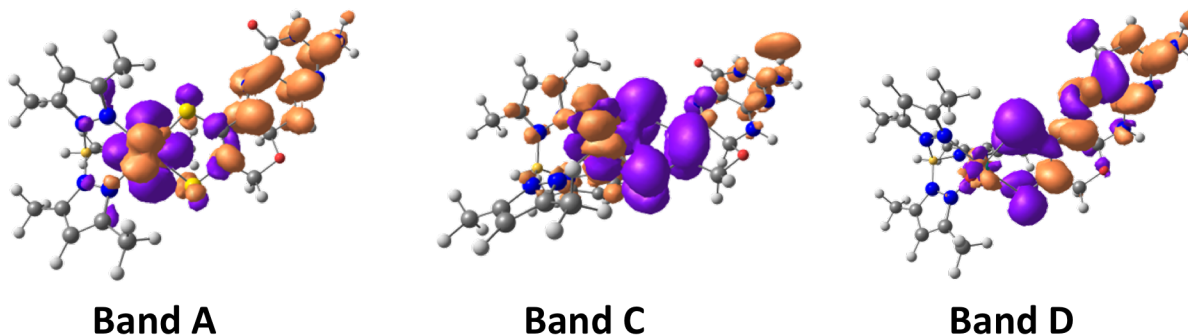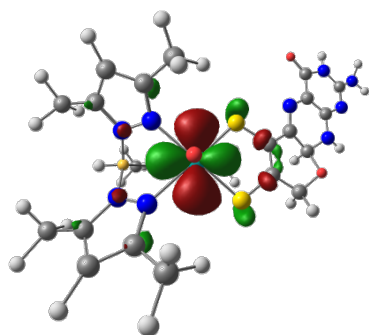
HOMO   LUMO
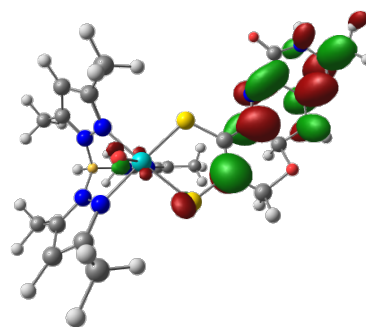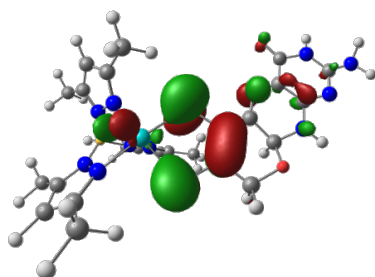
HOMO-1   HOMO-2
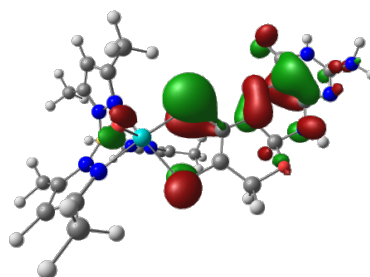
Figure S12. Resonance Raman profiles for <mark>2</mark>.
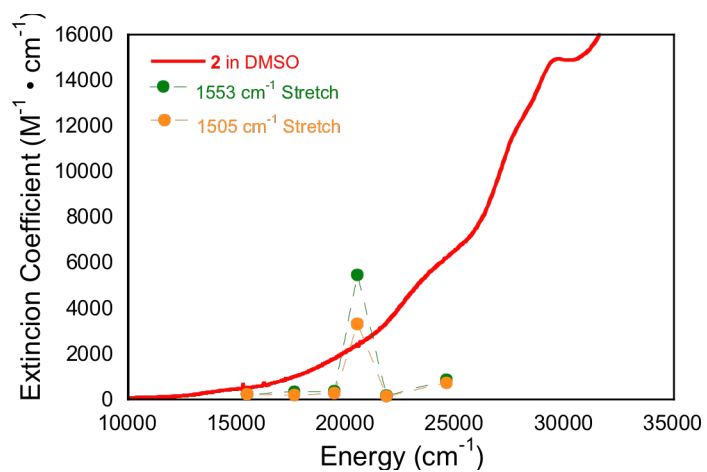
Figure S13. Experimental and computed resonance Raman spectra for **1.** A 0.975 scaling factor has been applied to the computed vibrational frequencies.
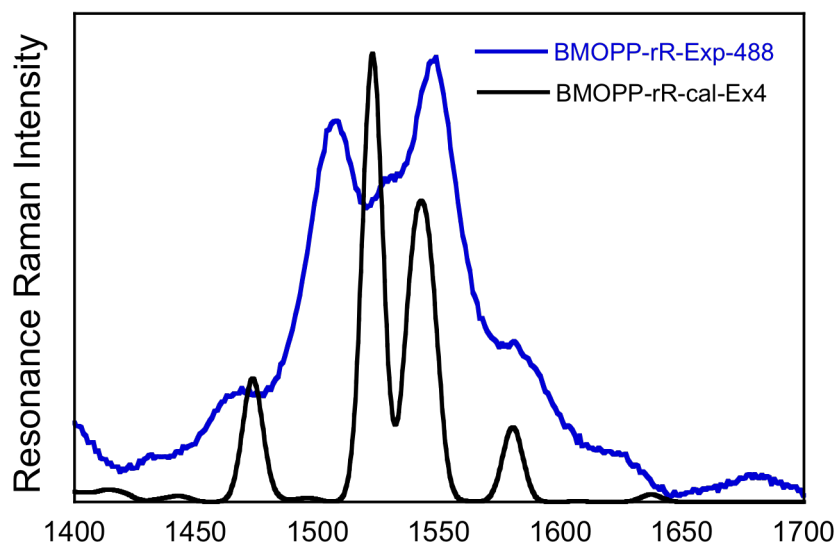
Figure S14. Experimental and computed HRESI (-) spectra for **2**. (Top) Experimental HRESI (-) of compound **2**. (Bottom) Calculated HRESI spectrum for [M-] as C32H42O3N11BMoS2.
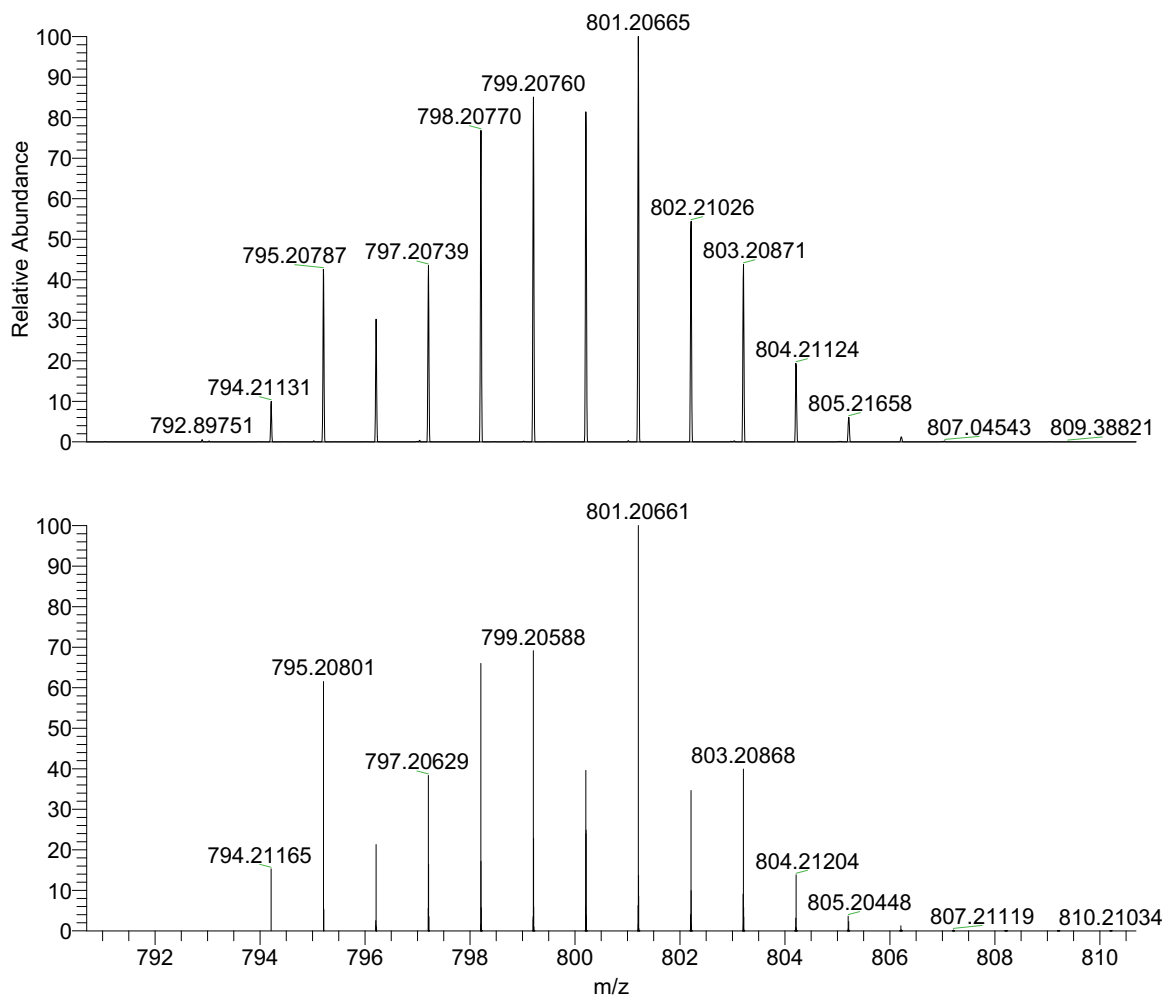
Figure S15. (Top) Mo K-edge Fourier transform of the EXAFS data for **1** and best fit to the data. (Bottom) Mo K-edge Fourier transform of the EXAFS data for **2** and best fit to the data. Data have been phase corrected using Mo-oxo backscattering.
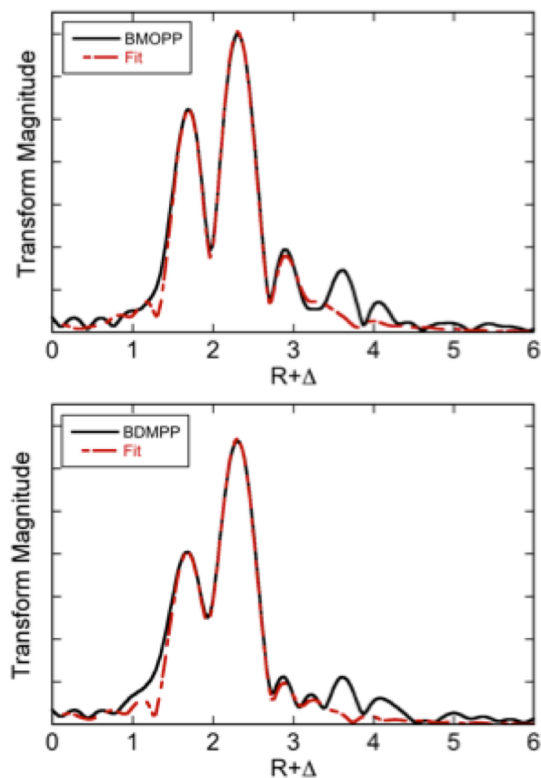
Table S3. Mo K-edge EXAFS best-fit parameters comparing **1** and **2**

	[TEA][Tp*Mo(O)(S₂BMOPP)] **1**				[TEA][Tp*Mo(O)(S₂BDMPP)] **2**		
	N	R (Å)	σ^2 (Å²)		N	R (Å)	σ^2 (Å²)
Mo-O	1	1.677	0.001	Mo-O	1	1.677	0.002
		[1.645(7)]					
Mo-S	2	2.370	0.003	Mo-S	2	2.339	0.003
		[2.370(3)]					
Mo-N(eq)	2	2.268	0.017	Mo-N(eq)	2	2.254	0.016
		[2.184(9)]					
Mo-N (bottom)	1	2.696	0.002	Mo-N (bottom)	1	2.620	0.001
		[2.399(9)]					
Mo-C/N	6	3.292	0.008	Mo-C/N	6	3.233	0.012
ΔE (eV)		-4.292				-6.594	
R%		5.92				6.53	

The bond distances for the x-ray structure of **1** are given in brackets. Fourier transformed EXAFS modulations for these compounds are presented in Fig. S14. The EXAFS for both **1** and **2** are dominated by two main backscattering interactions with transform peaks at R+Δ ~1.68 Å and ~2.35 Å. These are assignable as arising from Mo-oxo and Mo-S scatters, respectively. The analysis of the data reveals that **1** and **2** have nearly identical 6-coordinate $MoOS_2N_3$ first coordination spheres with compound **2** possessing slightly shorter Mo-S bond lengths (~0.03 Å). The EXAFS results are summarized in Table 1, and show excellent agreement with DFT computed bond lengths for geometrically optimized structures.

Analysis of S K-edge XAS Data. To quantitate the amount of S p orbital character in the low-energy 1s → ψ^* type transitions that comprise pre-edge Bands A and B, we define the total S 3p orbital character per hole (α^2) that contribute to the intensity of these pre-edge peaks using the equation,

$$D_0 = \frac{h}{3N}\alpha^2 I_{s(1s\to3p)} \quad (1)$$

Here, D_0 is the integrated area under a given pre-edge peak, h is the number of holes, N is the number of absorbers (N = 2 for a dithiolene ligand), and $I_{s(1s\to3p)}$ is the dipole integral for a 1s → 3p transition. We adopt a value of I_s = 11 for both the dithiolene ligands in **1** and **2** using previous published XAS data that relates the magnitude of the dipole integral with the S 1s → 4p transition energy position.[1] To determine the integrated areas of the pre-edge peaks for **1** and **2**, an arctangent function was fit to the step edge peaks and pseudo-Voigt functions were fit to the pre-edge region (Fig. 13). The integrated areas for pre-edge Bands A, B, and C are thus determined to be 0.08, 0.14, and 0.81 for **1**, and 0.06, 0.38, and 1.32 for **2**, respectively.

The LUMO of compound **1** possesses two holes (h = 2). Using Eqn. 1 with h = 2 we obtain α^2 = 0.022, or 2.2% S character per hole for this pterin-dithiolene based LUMO. Similarly, for **2** we use h = 4, since there are two pterin based LUMO orbitals, and obtain α^2 = 0.008, or 0.8% S character per hole. Thus, the total S character present in the pterin LUMO of **1** (2.2% total S) compared with the two pterin LUMOs of **2** (1.6% total S) shows that the S character in these pterin-based ILCT acceptor orbitals is small. In our analysis of Band B, we use h = 4 to obtain α^2 = 0.019, or 1.9% S character per hole (3.8% total for the (xz,yz) pair) for the Mo(xz,yz) orbitals of **1**. This compares with 5.2% S character per hole (10.4% for the (xz,yz) pair) for the Mo(xz,yz) orbitals of **2**.

Resonance Raman Frequency Assignments. In order to assign the most intense high frequency Raman vibrations (~1,450 – 1,600 cm^{-1}) and confirm the ILCT assignment for absorption band B in **1**, we have collected resonance Raman excitation profiles for the 1508 cm^{-1} and 1549 cm^{-1} Raman bands in **1** (Fig. 6) and the related 1505 cm^{-1} and 1553 cm^{-1} Raman bands in **2** (Fig. S13). Excitation at 488 nm pumps the low energy envelope of the dithiolene → pterin ILCT transition in **1**, resulting in resonance enhancement of normal modes that characterize the nature of the ILCT excited state distortion relative to the ground state geometry. We have computed the resonance Raman spectra for **1** (Figure S14) by setting the theoretical excitation energy to be equal to the TDDFT calculated transition energy for absorption band B. Large resonance enhancements were computed for computed vibrations at 1520 cm^{-1} and 1544 cm^{-1} in **1**, which correspond to resonantly enhanced experimental vibrational modes observed at 1508 cm^{-1} and 1549 cm^{-1}, respectively (Figure 10). The strong correlation between computed and experimental resonantly enhanced vibrations yields λ = 0.975 as the effective scaling factor for all the high frequency modes in the ~1,450 – 1,600 cm^{-1} region.

Using the λ = 0.975 frequency scaling factor and making use of the computed resonance Raman intensities and frequencies for **1**, the two most enhanced vibrations observed on resonance with absorption band B are assigned as (1) a pterin-dithiolene stretching modes that possess dominant dithiolene C=C stretch and pterin (pyrazine) C=N stretch character (1508 cm^{-1}), and (2) a pterin-dithiolene mode with dominant dithiolene C=C stretch and pterin (pyrimidine) C=N stretch character (1549 cm^{-1}) (Fig. 10). We are also able to confidently assign the 1467 cm^{-1} vibration as a pterin ring mode with both C=N and C=C motions and the 1580 cm^{-1} vibration as a pterin mode with C=C stretching character.

The strong resonance Raman enhancement of vibrational modes with pterin-dithiolene C=C and C=N character that are observed with excitation into absorption band B is fully consistent with the assignment of this band as a (HOMO-1) dithiolene → LUMO (pterin) ILCT transition. This one-electron promotion results in electron density being removed from the dithiolene HOMO-1, which possesses C=C π bonding character, and placed in a pterin LUMO with dominant C=C and C=N π* antibonding character. The resonance enhancement pattern also supports our assignment of absorption band A (Figure 6) as possessing (HOMO) Mo(x^2-y^2) → LUMO (pterin) MLCT character. The HOMO orbital of **1** is the doubly occupied Mo(x^2-y^2) orbital, which possesses small degree of C=C pseudo-σ bonding character, and as a result weaker resonance enhancement of both the 1508 cm^{-1} (C=C) and 1549 cm^{-1} (C=C) modes is observed when exciting in resonance with absorption band A. The resonance Raman profile for **2** shows resonance enhancement of the 1505 cm^{-1} and 1553 cm^{-1} modes with excitation at 488nm (Fig.

S13). Our DFT frequency calculations allow the 1505 cm^{-1} and 1553 cm^{-1} bands to be assigned as to modes that possess dithiolene C=C and pterin C=N/C=C stretching character with mode descriptions that essentially parallel those for **1**. Resonance enhancement of the 1505 cm^{-1} and 1553 cm^{-1} bands, coupled with the similarity in appearance for the Raman spectra of **1** and **2**, indicates dithiolene → pterin charge transfer character is also present in the charge transfer bands of **2**.

1.   Sarangi, R.; George, S. D.; Rudd, D. J.; Szilagyi, R. K.; Ribas, X.; Rovira, C.; Almeida, M.; Hodgson, K. O.; Hedman, B.; Solomon, E. I., Sulfur K-edge X-ray absorption spectroscopy as a probe of ligand-metal bond covalency: Metal vs ligand oxidation in copper and nickel dithiolene complexes. *J. Am. Chem. Soc.* **2007,** *129* (8), 2316-2326.